Human Pathology (2019) **86**, 170–181

ELSEVIER

Human PATHOLOGY

www.elsevier.com/locate/humpath

Original contribution

# Beyond sequence variation: assessment of copy number variation in adult glioblastoma through targeted tumor somatic profiling☆,☆☆

**Samantha N. McNulty PhD[a], Catherine E. Cottrell PhD[b], Katinka A. Vigh-Conrad PhD[a], Jamal H. Carter MD[c], Jonathan W. Heusel MD, PhD[a,d], George Ansstas MD[e], Sonika Dahiya MD[a,*]**

[a]*Department of Pathology and Immunology, Washington University School of Medicine, St Louis, MO 63110*
[b]*Institute for Genomic Medicine, Nationwide Children's Hospital, Columbus, OH 43205*
[c]*Department of Transfusion Medicine, Clinical Center, National Institute of Health, Bethesda, MD 20892*
[d]*Department of Genetics, Washington University School of Medicine, Saint Louis, MO 63110*
[e]*Department of Medicine, Division of Oncology, Washington University School of Medicine, St Louis, MO 63110*

Received 10 September 2018; revised 6 December 2018; accepted 14 December 2018

**Keywords:**
Glioblastoma;
Next-generation sequencing;
Clinical sequencing;
Copy number variation;
*EGFR* amplification

**Summary** Glioblastoma is the most common primary malignancy of the adult central nervous system. Gliomagenesis involves a complex range of alterations, including sequence changes, copy number variations (CNVs), and epigenetic modifications, that have clinical implications for disease classification and prognosis. Thus, multiple testing modalities are required to support a complete diagnostic workup. The goal of this study was to streamline the multipart workflow by predicting both sequence changes and CNVs (specifically *EGFR* amplifications) from a single next-generation sequencing (NGS) test. Eighty-six primary and secondary glioblastomas were submitted for clinical NGS to report sequence variants from a concise panel of cancer-relevant genes. Most specimens underwent concomitant testing by methylation-specific polymerase chain reaction, immunohistochemistry, and fluorescence in situ hybridization. Using data generated during the course of clinical testing, we found that NGS-based variant predictions were concordant with immunohistochemistry and fluorescence in situ hybridization for *IDH* mutation and *EGFR* amplification status, respectively. We also noted that *EGFR* amplifications correlated with polysomy of chromosome 7, 19, and 20, and loss of *PTEN* and *CDKN2A*. *EGFR*-unamplified cases had lower rates of chromosome 7 polysomy, and *PTEN* and *CDKN2A* loss, but more CNVs overall. *TP53*, *NF1*, *ATRX*, and *PDGFRA* mutations were nearly exclusive to specimens without *EGFR* amplification. *EGFR* amplification was not associated with longer progression-free survival in this cohort, but amplifications were enriched in a group with slightly longer overall survival despite radiographic evidence of disease progression. Further study is needed to explore the mechanisms responsible for noted patterns of co-occurring variants and to correlate them with specific clinical outcomes.

☆ Competing interests: The authors confirm that they have no conflicts of interest. All experiments were performed according to relevant legal and ethical regulations.

☆☆ Funding/Support: This study was supported by research funds from the Division of Neuropathology, Department of Pathology and Immunology, Washington University School of Medicine (St Louis, MO).

* Corresponding author at: Department of Pathology and Immunology, Washington University School of Medicine, 660 S. Euclid Avenue, St Louis, MO 63110.

https://doi.org/10.1016/j.humpath.2018.12.004

## 1. Introduction

Glioblastoma (GBM, World Health Organization [WHO] grade IV) is the most common cancer of the adult central nervous system (CNS), accounting for ~15% of primary and 46% of malignant CNS tumors [1]. GBM patients have a poor prognosis, with median survival of >15 months. The standard regimen of surgical resection, radiation, and chemotherapy has not changed significantly in decades, and targeted treatments have shown little benefit considering the GBM population as a whole [2].

Various next-generation sequencing (NGS) studies have described the mutational landscape of GBM [3-5], which includes complex combinations of single nucleotide variants (SNVs), insertions/deletions (indels), copy number variations (CNVs), and epigenetic modifications. Some of these findings led to further diagnostic and prognostic stratification of gliomas. For instance, activating mutations in isocitrate dehydrogenase 1 and 2 (*IDH1* ;and *IDH2*) genes distinguish primary (IDH wild-type, *IDHwt*) from secondary GBMs, the latter evolving from lower-grade glioma and carrying a better prognosis [4,6]. Telomerase reverse transcriptase (*TERT*) promoter variants were also associated with poor outcome [4,7], but the implications of other recurrent variants (eg, mutations in *TP53, PTEN, EGFR, NF1, PIK3CA*) have yet to be elucidated.

Amplification of the epidermal growth factor receptor (*EGFR*) is common in GBM and is often assessed during the diagnostic workup despite uncertain prognostic value. Some studies showed little correlation between *EGFR* amplification and factors such as response to treatment or overall survival (OS), whereas others drew opposing conclusions [8-12]. Many of these studies were performed before molecular features were incorporated into clinical diagnosis. Thus, it is necessary to revisit these surveys in light of the updated classification schema to identify distinct subgroups with unique survival or drug response outcomes.

The initial aim of this study was to determine whether the diverse variants that are significant in GBM could be assessed with a single hybridization capture-based NGS assay. Eight-six consecutive GBMs were submitted for NGS testing to detect SNVs and indels in a concise set of genes specifically relevant to CNS tumors. Most specimens were also sent for other molecular tests, such as immunohistochemistry (IHC), fluorescence in situ hybridization (FISH), and methylation-specific polymerase chain reaction (PCR), for a complete pathological workup. Using FISH data as a comparator, we showed that we could accurately predict CNVs in *EGFR* (and the rest of the genome) using our clinical NGS assay. We also noted that *EGFR*-amplified and -unamplified cases show disparate patterns of sequence variants, CNVs, and possibly even clinical outcomes. Further work is however required to determine the molecular mechanisms responsible for these patterns and to ascertain their greater significance.

## 2. Materials and methods

### 2.1. Biological materials

Eighty-six consecutive formalin-fixed, paraffin-embedded (FFPE) GBMs were submitted to Genomics and Pathology Services at Washington University in St Louis (GPS@WUSTL, https://gps.wustl.edu) for testing via the CCGSv3.1 CNS Tumor Gene Set (Supplementary Table S1) between April 22, 2015, and May 25, 2016. All cases were initially reviewed by board-certified neuropathologists according to the WHO 2007 guidelines for classification of tumors of the CNS [13] prior to sequencing and were later reviewed per revised WHO 2016 schema.

### 2.2. DNA preparation and NGS

NGS testing was performed as previously described [14]. FFPE blocks were examined by board-certified neuropathologists to identify regions with sufficient neoplastic cellularity. Cores were punched from marked areas, and DNA was isolated using a Qiagen QIAamp DNeasy Blood and Tissue Kit (Qiagen, Hilden, Germany). Input ranged between 50 and 750 ng genomic DNA. DNA was sonicated to achieve 140-230 base pair (bp) fragments with a Covaris Ultrasonicator (Woburn, MA) and assessed by an Agilent Bioanalyzer 2100 (Agilent, Santa Clara, CA). NGS libraries were prepared with the KAPA Hyper Prep Kit (KAPA Biosystems, Wilmington, MA) and amplified via limited cycle PCR. A total of 500 ng of library was hybridized to custom cDNA capture probes for 16-18 hours. The 390-kilobase capture space encompasses all coding exons of 131 cancer-relevant genes (Supplementary Table S1); select introns encompassing hotspots for rearrangement breakpoints; and dispersed, intergenic regions included for quality control. The hybridized product was washed and amplified using primers from the KAPA amplification kit (KAPA Biosystems). Captured libraries were pooled and sequenced on an Illumina HiSeq2500 (Illumina, San Diego, CA) to generate 2 × 101 bp paired-end reads.

### 2.3. Preprocessing and read alignment

Raw base call files were converted to fastq format using Cassava v1.8 (Illumina) and demultiplexed using in-house

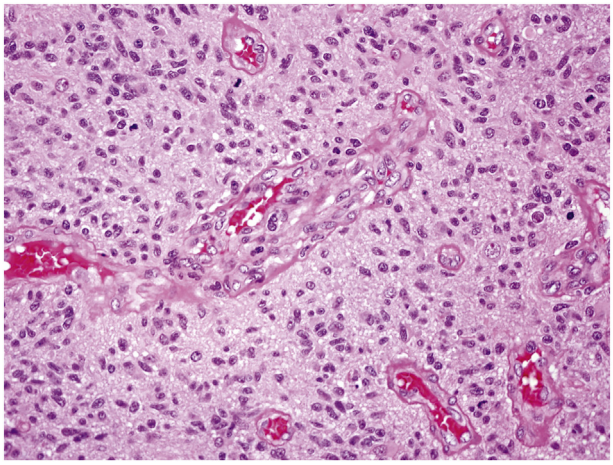

**Fig. 1** Microscopic appearance of GBM. Representative hematoxylin and eosin–stained image from a GBM patient with *EGFR* amplification. Salient features herein include dense cellularity, brisk mitotic activity, and microvascular proliferation.

scripts. Paired-end reads were aligned to the human reference (UCSC hg19, NCBI build 37.2, NCBI RefSeq annotation v37.2) with Novoalign v3.02 (Novocraft Technologies, Selangor, Malaysia). Alignment files were converted to BAM format with samtools v0.1.19 [15], and duplicate reads were marked using Picard Tools MarkDuplicates v1.53 (https://broadinstitute.github.io/picard/). Cases had an average total count of 30.9 ± 8.8 million reads and an average 11.4 ± 3.5 million high-quality reads uniquely mapped to the targeted regions (Supplementary Fig. S1).

## 2.4. Prediction of SNVs and small indels

SNVs were called using SAMtools mpileup v0.1.19 [15,16] and VarScan2 v2.3.6 [17] with the following cutoffs: depth ≥50 reads, base quality ≥20, mapping quality ≥30, Fisher strand bias ≤75, and variant allele fraction >3% [14]. Indels <21 bp were predicted using Unified Genotyper from the Genome Analysis Toolkit v1.2 [18] with the following cutoffs: depth ≥50 reads, Fisher strand bias ≤75, and homopolymer

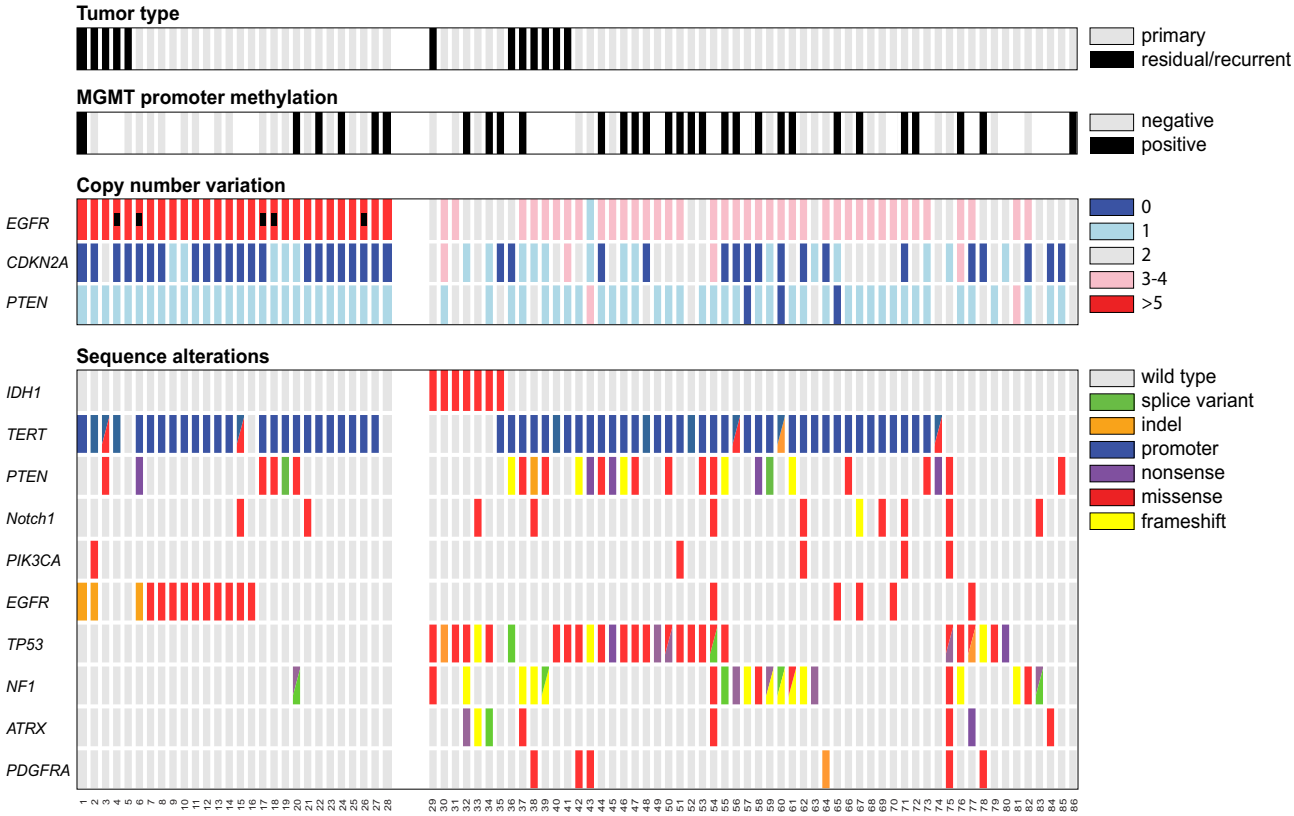


**Fig. 2** Copy number and nonsynonymous sequence variation in GBM. The various genomic alterations present in each GBM specimen are shown. Black boxes indicate residual/recurrent GBM and specimens that tested positive for MGMT promoter methylation in the respective rows. White boxes indicate that the specimen was not tested. Copy number losses (blue) and gains (red) were determined from sequencing data. Black squares within the *EGFR* row denote cases with the *EGFRvIII* deletion (ie, deletions of exons 2-7 within the amplified gene). Various nucleotide sequence changes were recorded from sequencing data; common polymorphisms were excluded. The specific nomenclature describing each alteration is available in Supplementary Table S2.

**Table 1** Pathologic and demographic features of study cases

| Case | Sex | Age | Original diagnosis (2007 WHO) | Revised diagnosis (2016 WHO) | Secondary | Residual/ recurrent |
|---|---|---|---|---|---|---|
| 1 | Female | 48 | GBM | | | X |
| 2 | Female | 64 | Small cell GBM | | | X |
| 3 | Female | 67 | GBM with treatment effect | | | X |
| 4 | Female | 62 | GBM | | | X |
| 5 | Male | 63 | GBM with treatment effect | | | X |
| 6 | Male | 59 | GBM | | | |
| 7 | Female | 49 | Small cell GBM | | | |
| 8 | Male | 53 | Small cell GBM | | | |
| 9 | Male | 51 | GBM | | | |
| 10 | Male | 59 | GBM | | | |
| 11 | Male | 61 | GBM | | | |
| 12 | Male | 62 | GBM | | | |
| 13 | Male | 55 | OA | AA with molecular GBM findings | | |
| 14 | Male | 55 | Small cell GBM | | | |
| 15 | Female | 59 | GBM | | | |
| 16 | Male | 54 | Small cell GBM | | | |
| 17 | Male | 56 | GBM with small cell features | | | |
| 18 | Female | 56 | GBM | | | |
| 19 | Male | 61 | GBM | | | |
| 20 | Female | 55 | GBM | | | |
| 21 | Male | 73 | GBM | | | |
| 22 | Male | 83 | GBM | | | |
| 23 | Male | 66 | Small cell GBM | | | |
| 24 | Female | 60 | GBM | | | |
| 25 | Male | 73 | Small cell GBM | | | |
| 26 | Male | 61 | GBM | | | |
| 27 | Male | 74 | GBM with small cell features | | | |
| 28 | Female | 72 | GBM | | | |
| 29 | Female | 49 | GBM with focal primitive neuronal component and treatment effect | GBM, IDH mutant, with focal primitive neuronal component and treatment effect | X | X |
| 30 | Female | 31 | GBM | GBM, IDH mutant | X | |
| 31 | Male | 53 | GBM with PNET characteristics | GBM, IDH mutant, with primitive neuronal component | X | |
| 32 | Male | 58 | GBM with oligodendroglial component | GBM, IDH mutant | X | |
| 33 | Male | 34 | GBM with treatment effect | GBM, IDH mutant | X | |
| 34 | Female | 36 | GBM | GBM, IDH mutant | X | |
| 35 | Female | 59 | GBM | GBM, IDH mutant | X | |
| 36 | Male | 70 | GBM | | | X |
| 37 | Male | 74 | GBM | | | X |
| 38 | Male | 57 | GBM with treatment effect | | | X |
| 39 | Female | 26 | GBM with treatment effect | | | X |
| 40 | Female | 54 | GBM with treatment effect | | | X |
| 41 | Male | 46 | Persistent/recurrent GBM | | | X |
| 42 | Male | 57 | GBM with primitive neuroectodermal and sarcomatous components | | | |
| 43 | Female | 73 | GBM | | | |
| 44 | Male | 69 | GBM | | | |
| 45 | Female | 62 | GBM with primitive neuronal component | | | |
| 46 | Female | 81 | GBM | | | |
| 47 | Male | 51 | GBM | | | |
| 48 | Male | 74 | GBM | | | |
| 49 | Female | 72 | GBM | | | |
| 50 | Male | 67 | GBM | | | |

**Table 1** (*continued*)

| Case | Sex | Age | Original diagnosis (2007 WHO) | Revised diagnosis (2016 WHO) | Secondary | Residual/ recurrent |
|---|---|---|---|---|---|---|
| 51 | Female | 65 | GBM | | | |
| 52 | Male | 61 | GBM with giant cell and PNET features | GBM with giant cell and primitive neuronal components | | |
| 53 | Male | 58 | GBM | | | |
| 54 | Male | 56 | GBM | | | |
| 55 | Female | 54 | GBM | | | |
| 56 | Male | 53 | GBM | | | |
| 57 | Male | 60 | GBM | | | |
| 58 | Male | 83 | GBM | | | |
| 59 | Female | 40 | GBM | | | |
| 60 | Female | 66 | GBM | | | |
| 61 | Male | 79 | GBM | | | |
| 62 | Male | 62 | GBM | | | |
| 63 | Female | 77 | GBM | | | |
| 64 | Male | 73 | GBM | | | |
| 65 | Male | 58 | GBM | | | |
| 66 | Male | 54 | GBM | | | |
| 67 | Male | 60 | OA with focal anaplasia | AA with molecular GBM findings | | |
| 68 | Male | 64 | GBM | | | |
| 69 | Male | 67 | GBM | | | |
| 70 | Female | 77 | AA | AA with molecular GBM findings | | |
| 71 | Female | 60 | GBM | | | |
| 72 | Male | 57 | GBM | | | |
| 73 | Female | 53 | AA | AA with molecular GBM findings | | |
| 74 | Female | 69 | GBM with focal primitive neuronal differentiation | | | |
| 75 | Male | 45 | GBM | | | |
| 76 | Female | 56 | GBM | | | |
| 77 | Female | 23 | GBM | | | |
| 78 | Male | 62 | GBM with prominent primitive neuronal component | | | |
| 79 | Female | 71 | GBM | | | |
| 80 | Female | 80 | OA | GBM | | |
| 81 | Female | 38 | OA | GBM | | |
| 82 | Male | 66 | GBM with focal sarcomatoid features | | | |
| 83 | Female | 66 | AA | AA with molecular GBM findings | | |
| 84 | Female | 37 | GBM | | | |
| 85 | Male | 46 | GBM | | | |
| 86 | Female | 80 | GBM | | | |

Abbreviation: AA, anaplastic astrocytoma; OA, anaplastic oligoastrocytoma; PNET, primitive neuroectodermal tumor.

runs <7 bp. Reporting was restricted to the CNS Tumors Gene Set (marked in Supplementary Table S1). The clinical relevance of the identified variants was determined as described previously [19]. Common polymorphisms found in population databases (eg, Exome Aggregation Consortium and Genome Aggregation Database [20]) were excluded from this report.

## 2.5. Copy number assessment

CNVs were inferred using CNVkit [21], a software designed to assess $\log_2$ copy ratios from targeted capture NGS data based on reads mapped to both on-target and off-target regions. Fifteen clinical FFPE specimens derived from a variety of nonmalignant disease associations were used as an averaged control to normalize read coverage for this assay. Control samples were devoid of CNVs on the basis of allele frequency plots generated during routine analysis and an orthogonal NGS-based CNV prediction tool (CopywriteR [22]). Control and test cases were processed through CNVkit's standard batch pipeline using the alignment files generated for SNV/indel prediction (see above). By default, the on-target bin size was set to 267 bp and off-target bin size was adjusted to

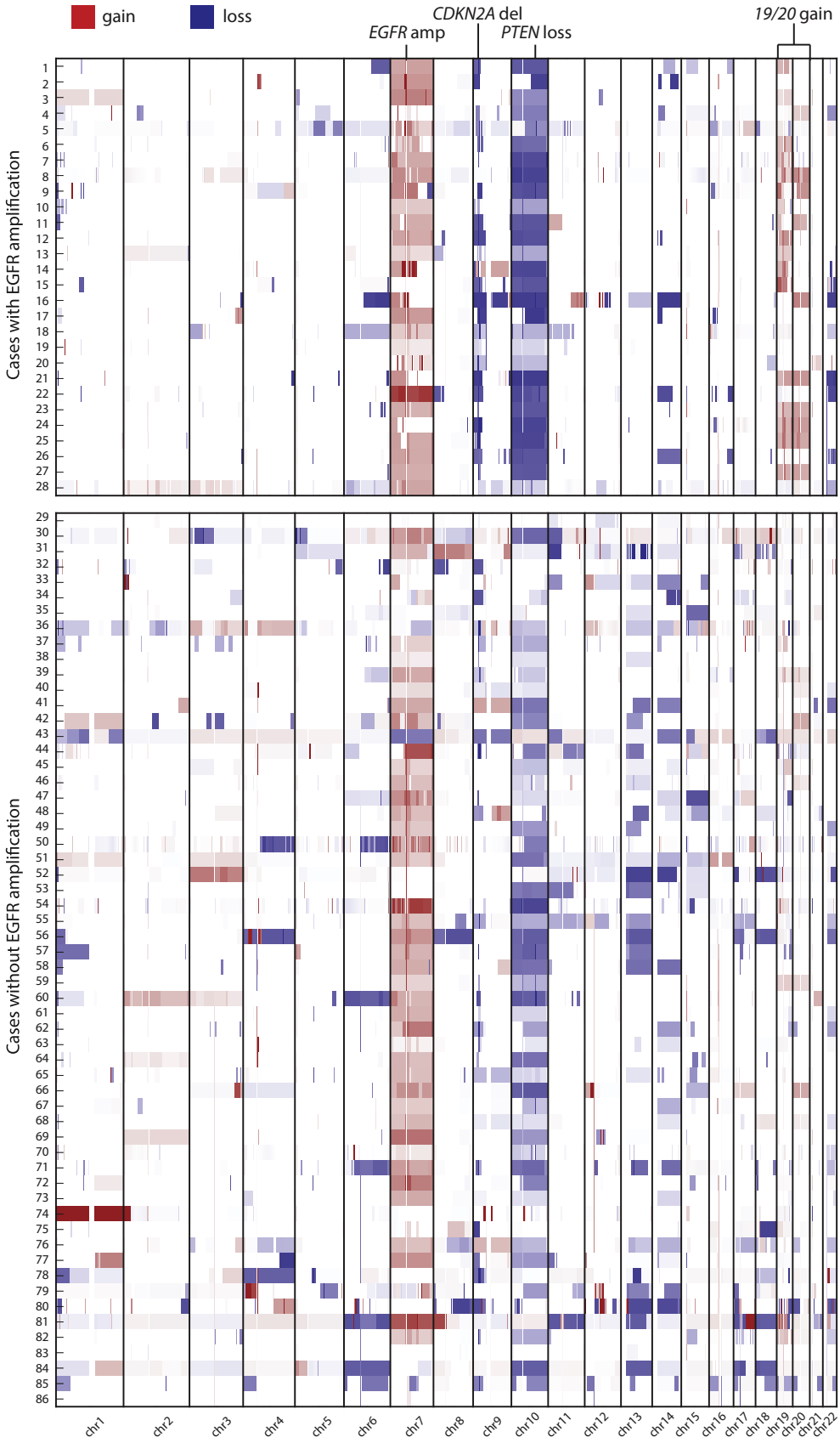
gain
loss
*EGFR* amp
*CDKN2A* del
*PTEN* loss
*19/20* gain
Cases with EGFR amplification
Cases without EGFR amplification
chr1
chr2
chr3
chr4
chr5
chr6
chr7
chr8
chr9
chr10
chr11
chr12
chr13
chr14
chr15
chr16
chr17
chr18
chr19
chr20
chr21
chr22

**Table 2** Variant rates among *EGFR*-amplified and -unamplified cases

| Variant | *EGFR*-amplified (n = 28) | *EGFR*-unamplified (n = 60) | All cases (N = 86) |
|---|---|---|---|
| Chr 7 polysomy | 23 (82.1%) | 40 (66.7%) | 63 (73.3%) |
| Chr 19 polysomy | 17 (60.7%) | 8 (13.3%) | 25 (29.1% |
| Chr 20 polysomy | 10 (35.7%) | 7 (11.7%) | 17 (19.8%) |
| Chr 10 loss | 27 (96.4%) | 42 (70.0%) | 68 (79.1%) |
| Chr 13 loss | 1 (3.6%) | 26 (43.3%) | 27 (31.4%) |
| Chr 14 loss | 5 (17.9%) | 17 (28.3%) | 22 (25.6%) |
| *PTEN* loss | 28 (100.0%) | 43 (71.7%) | 71 (82.6%) |
| *CDKN2A* loss | 27 (96.4%) | 31 (51.7%) | 58 (67.4%) |
| *CDK4* amplification | 3 (10.7%) | 11 (18.3%) | 14 (16.3%) |
| *PDGFRA* amplification | 0 (0.0%) | 10 (16.7%) | 10 (11.6%) |
| *KIT* amplification | 1 (3.6%) | 9 (15.0%) | 10 (11.6%) |
| *KDR* amplification | 0 (0.0%) | 7 (11.7%) | 7 (8.1%) |
| *MET* amplification | 0 (0.0%) | 1 (1.7%) | 1 (1.2%) |

achieve approximately equal read counts in on- and off-target bins. The average off-target bin size across the 86 cases was 99.1 ± 8.6 kilobases. The on- and off-target read depths were then combined and normalized to the averaged control, and $\log_2$ copy number profiles were generated. A circular binary segmentation algorithm was run on the $\log_2$ ratios to join related bins into larger segments. Copy number was estimated from the both the bin and segmentation data with tumor purity conservatively set to 100%. A custom script was used to calculate the total length of segments that deviate from a 2-copy state. Polysomies were noted when a chromosome was found at >2 copies, whereas focal amplifications were called when a specific gene/locus was estimated at >5 copies and in excess of the surrounding region.

## 2.6. Fluorescence in situ hybridization

FFPE blocks were sectioned to 5 $\mu$m and mounted on slides. Sections were deparaffinized in CitriSolv, dehydrated in 100% ethanol, pretreated, and pepsin digested using reagents from the Paraffin Pretreatment Reagent Kit II (Abbott Molecular, Abbott Park, IL). Slides were dehydrated in ethanol and dried prior hybridization overnight with probes from the Vysis *EGFR*/CEP7 FISH probe kit (Abbott Molecular). Hybridized slides were washed in 2× SSC/0.3%NP-40 for 2 minutes at 74°C and then at room temperature for 1 minute, air dried, and counterstained with DAPI II. Results were viewed under a BX61 fluorescent microscope (Olympus, Melville, NY) and photographed using the Jai Progressive Scan camera and CytoVision Imaging System (Leica Biosystems, Wetzlar, Germany). Typically, 200 interphase nuclei were examined in each specimen. Ratios of signal from locus-specific and chromosome-enumerating probes were determined to call polysomies, monosomies, and focal gains and losses.

## 2.7. Immunohistochemistry

FFPE blocks were sectioned to 5 $\mu$m and affixed to slides. Sections were deparaffinized and rehydrated according to standard histological methods and labeled with antibodies using the Benchmark Ultra automated slide staining system (Ventana Medical Systems, Inc, Tucson, AZ). Monoclonal antibody against $IDH1^{R132H}$ (Dianova, Hamburg, Germany) was diluted 1:500 in Antibody Diluent (Dako, Carpinteria, CA). Parameters for slide processing were: antigen retrieval (36 minutes in Ultra CC1 mild, 1 mmol/L EDTA pH 8.0), primary antibody staining (37°C for 1 hour), washing (Ultrawash), and detection (ultraView Universal DAB Detection Kit; Ventana Medical Systems).

## 2.8. O6-methylguanine-DNA methyl-transferase methylation assay

Methylation of the O6-methylguanine-DNA methyltransferase (*MGMT*) promoter was assessed by methylation-specific PCR at a commercial laboratory (LabCorp, Burlington, NC) as previously described [23]. Briefly, DNA was isolated from FFPE specimens and treated with bisulfate to convert unmethylated cytosine to uracil, which is detectable via real-time PCR.

**Fig. 3** Genome-wide CNV in GBM. Copy number gains (red) and losses (blue) are plotted along the 22 autosomal chromosomes of the human genome. Whereas gains in chr 7 and losses of chr 10 and 9p are universally common, gains in chr 19 and 20 are more common in cases with *EGFR* amplification (cases 1-28), and losses of chr 13 and 14 are more common in cases without *EGFR* amplification (cases 29-68). Overall, cases without *EGFR* focal amplification appear to have more regions that deviate from a 2-copy state.

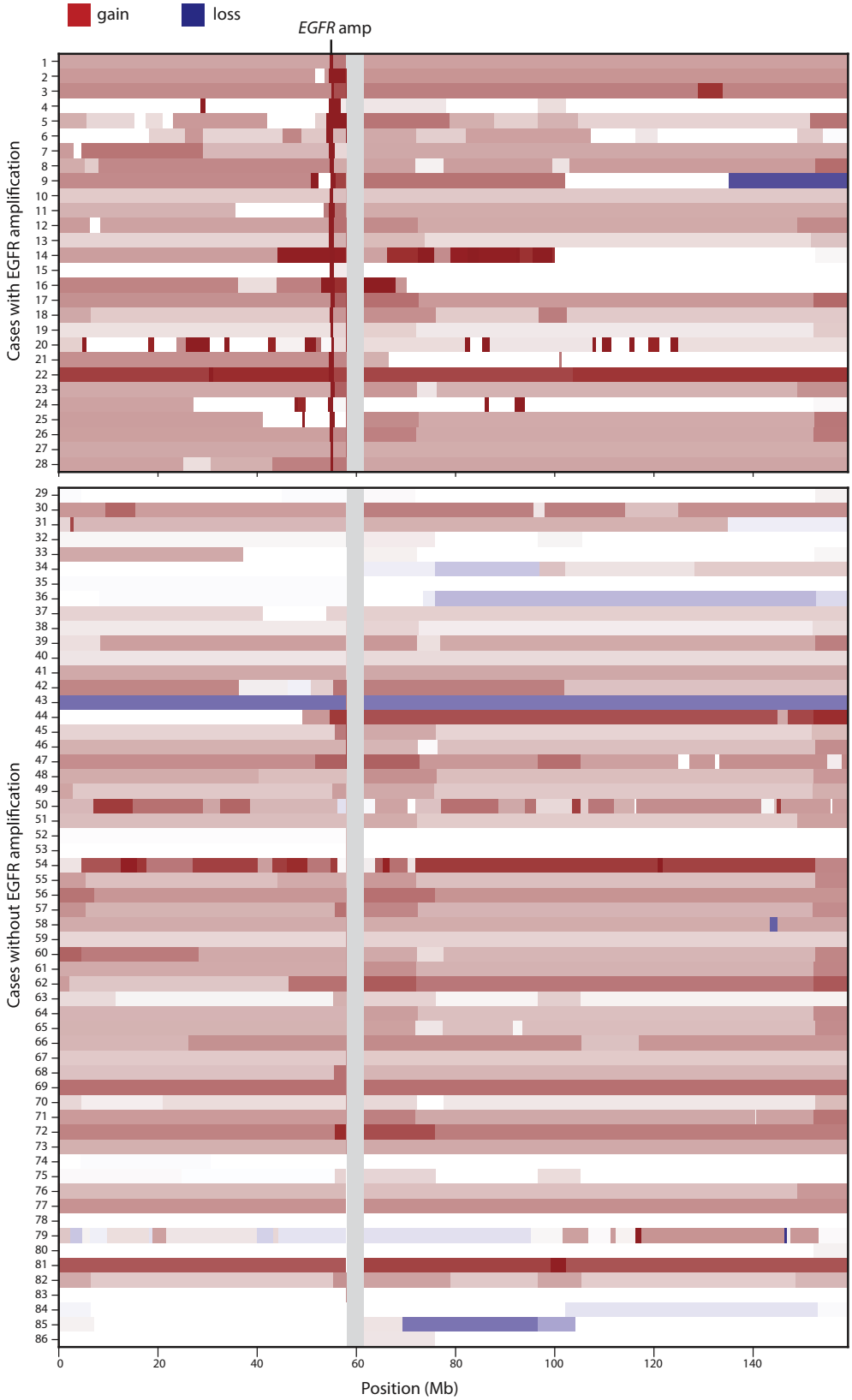


**Fig. 4** CNV along chr 7 in GBM. Copy number gains (red) and losses (blue) are plotted along chr 7 of the human genome. Most GBM cases included in this study show polysomy of chr 7, although the polysomy may or may not encompass the full length of the chromosome. Focal amplification of the region around *EGFR* (ie, estimated ≥5 copies) was noted in cases 1-28.

## 3. Results

### 3.1. Samples and clinical data

Eighty-six GBM specimens were submitted to GPS@WUSTL for targeted sequencing of the CNS Tumor Gene Set during the referenced time frame (Table 1, Supplementary Table S2). The original diagnosis, based on histological review according to WHO 2007 criteria (see Fig. 1 for example), is listed in Table 1 alongside a revised WHO 2016 classification where applicable. The 49 male and 37 female patients ranged from 23 to 83 years at the time of specimen collection. Twelve specimens were derived from residual or recurrent disease; others were collected at the time of initial diagnosis.

### 3.2. Nucleotide sequence variation

Nonsynonymous SNVs and indels found in the 24 genes of the CNS Tumor Gene Set were cataloged for each specimen (Fig. 2; see Supplementary Table S2 for exact syntax). Seven of the 86 specimens (8.1%) were classified as secondary GBM based on activating mutations in *IDH1* (Table 1), a rate consistent with previous reports [24]. NGS findings were 100% concordant with IHC for the canonical *IDH1* p.R132H mutation (Supplementary Table S2). NGS identified activating *IDH1* p.R132G mutations in 2 more cases. The 7 IDH-mutant (*IDHmut*) patients were, on average, younger than the *IDHwt* patients (Supplementary Fig. S2).

Activating *TERT* promoter mutations (c.-124C > T [C228T] and c.-146C > T [C250T]) were the most abundant SNV in this cohort (75.6% of cases). Although *TERT* promoter mutations are rare in *IDHmut* GBM [7], we identified 1 specimen with both *TERT* c.-124C > T [C228T] and *IDH1* R132H mutations. Other commonly altered genes included *PTEN* (32.6%), *TP53* (32.6%), *NF1* (24.4%), *EGFR* (20.9%), *NOTCH1* (9.3%), and *ATRX* (9.3%) (Fig. 2, Supplementary Table S2). With the exception of *NF1* mutations, which were noted in approximately 9% of GBMs in other cohorts, mutation rates within these genes were as expected [5,6]. Three cases showed SNVs in *BRAF* (Supplementary Table S2); one was a *BRAF* V600E mutation, a well-known, targetable mutation [25], albeit rare in adult GBM [3,26].

*ATRX* and *TERT* promoter mutations are considered mutually exclusive [7], but 2 specimens had mutations in both genes. In these cases, the *ATRX* mutations were not found in population databases (Exome Aggregation Consortium, Genome Aggregation Database, etc), nor were they previously associated with cancer (via COSMIC [27] or cBioPortal [28,29]). They were classified as variants of uncertain clinical significance and may represent rare polymorphisms rather than true somatic variants.

### 3.3. MGMT promoter methylation

*MGMT* is a DNA repair enzyme that can reduce the efficacy of alkylating drugs (eg, temozolomide). Methylation-based silencing of *MGMT*, a favorable indicator of temozolomide response, was assessed using methylation-specific PCR in 63 cases (Supplementary Table S2, Fig. 2). *MGMT* promoter (MGMTp) methylation was found in 47.5% of *IDHwt* GBMs. Previous studies have reported *MGMTp* methylation in a majority of *IDHmut* cases [30], but this was not the case in our cohort (Fig. 2). *MGMTp* methylation did not correlate with the other variants identified in this study.

### 3.4. CNV from NGS data

As expected [31], the most common CNVs found in our data set were polysomy of chromosome (chr) 7 and monosomy of chr 10, often co-occurring (Fig. 3). Gains/losses of chr 7 and chr 10 tended to span the entire chromosome. In contrast, chr 9 losses were mostly restricted to the p-arm (Fig. 3).

*CDKN2A* (chr 9p21) and *PTEN* (chr 10q23) loss was noted in 67.4% and 80.2% of cases, respectively, whereas *EGFR* (chr 7p11.2) amplification was noted in 32.6% of cases (Table 2, Figs. 3 and 4). *EGFR* amplification was restricted to *IDHwt* cases and often associated with SNVs in the amplified gene (Fig. 2).

Sixty-three cases were tested for *EGFR* amplification by FISH; results were concordant with NGS-based predictions in all but 2 cases for which the 2 assays were performed on separate specimen blocks (ie, different regions of the tumor). Thus, the discordance could be due to intratumor heterogeneity, a noted feature of GBM [32,33]. The *EGFRvIII* deletion

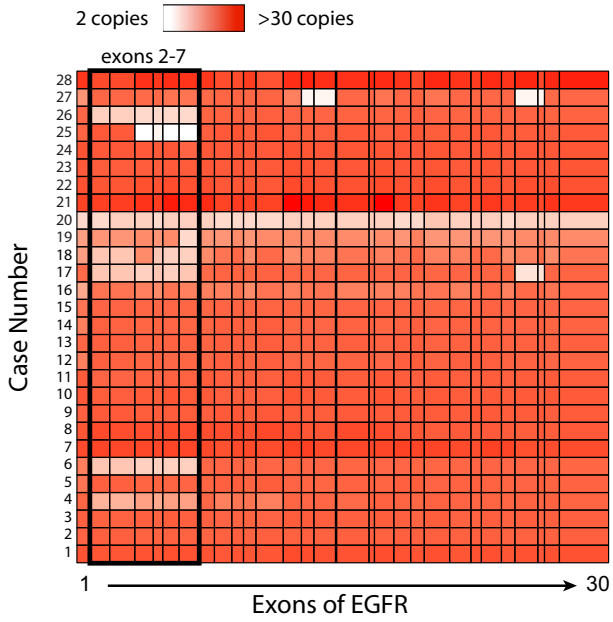


**Fig. 5** Detection of the *EGFRvIII* deletion in EGFR-amplified cases. Copy number was estimated for discrete exons of EGFR. The well-characterized *EGFRvIII* deletion, the deletion of exons 2-7 within an otherwise amplified locus, was detected in 5 of the 28 EGFR-amplified cases. Other deleted exons were noted; the clinical significance of these (if any) is unknown.

(ie, deletion of exons 2-7) was noted in 5 of the 28 amplified cases (Fig. 5), highlighting the resolution of NGS-based CNV prediction.

### 3.5. Disparate molecular profiles of *EGFR*-amplified versus unamplified cases

Broad differences were noted in the molecular profiles of *EGFR*-amplified versus unamplified specimens (Table 2, Fig. 2). *EGFR* amplification correlated with loss of *CDKN2A* and *PTEN* and polysomy of chr 7, 19, and 20. Cases without *EGFR* amplifications had more CNVs overall (Fig. 3) but lower rates of chr 7 polysomy, *CDKN2A* loss, and *PTEN* loss (Figs. 2 and 3, Table 2). Likewise, nonsynonymous point mutations were observed with greater frequency in specimens without *EGFR* amplification. Mutations in *TP53, NF1, ATRX,* and *PDGFRA* were nearly exclusive to the *EGFR*-unamplified cases (Fig. 2).

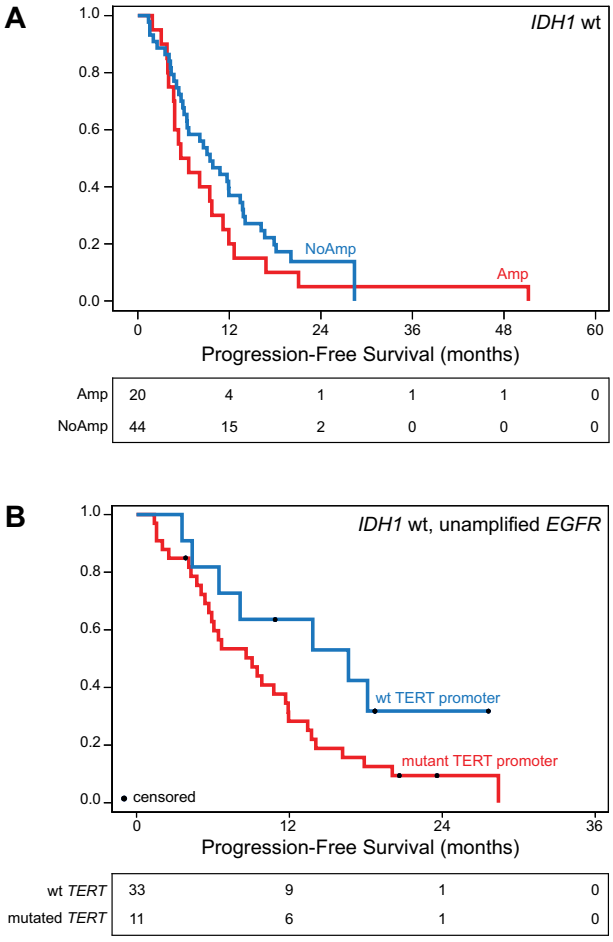


**Fig. 6** The impact of activating *IDH1* mutations and *EGFR* amplification on PFS. A, Kaplan-Meier plots indicate that there is no difference in PFS between *IDHwt* patients with and without *EGFR* amplification; log-rank $P = .232$. B, Among *IDHwt* patients without *EGFR* amplification, activating mutations in the *TERT* promoter were associated with somewhat shorter PFS compared to patients with wild-type *TERT* promoters; log-rank $P = .079$.

**Table 3** Disease progression and survival of patients with *IDH* wild-type, primary GBM with and without *EGFR* amplification

| | Amplified *EGFR* | Unamplified *EGFR* |
|---|---|---|
| Patients with medical record | 16 | 33 |
| Progression prior to death | 11 | 10 |
| No progression prior to death | 5 | 23 |
| Average OS | 68.1 ± 57.3 wk | 56.2 ± 30.0 wk |
| Average OS of patients with progression prior to death | 74.6 ± 67.7 wk | 76.4 ± 34.3 wk |
| Average OS of patients without progression prior to death | 53.8 ± 22.1 wk | 47.3 ± 23.6 wk |

### 3.6. *EGFR* amplification status and patient outcomes

Clinical follow-up data (including OS, progression-free survival [PFS] following radiation treatment, etc) was available for 71 patients (Supplementary Table S2). OS ranged from 6 to 506 weeks (average 73.4 ± 68.6 weeks), whereas PFS ranged from 6 to 478 weeks (average 65.5 ± 73.2 weeks).

As expected [4,5,34], the few *IDHmut* patients included in this study showed longer PFS compared to *IDHwt* patients in univariate survival analyses (log-rank $P = .0274$). Although there was no difference in the PFS of *IDHwt* patients with and without *EGFR* amplification (Fig. 6A), most patients with *EGFR* amplifications showed radiographic evidence of disease progression prior to death (Table 3). The average OS of *IDHwt* patients with noted disease progression events prior to death was longer compared to that of patients without noted progression despite similar age distributions. Although activating mutations in the *TERT* promoter were nearly ubiquitous in the group with *EGFR* amplifications, they showed a negative impact on PFS in *EGFR*-unamplified cases (Fig. 6B); this could account for the divergent OS outcomes seen in this subgroup.

## 4. Discussion

Genetic testing is a vital tool in the diagnosis and treatment of GBM. At present, a thorough characterization may include multiple assays (ie, FISH, IHC, methylation-specific PCR, NGS, etc) to assess all relevant genes. Here, we showed that a small, targeted NGS assay is capable of detecting many of the alterations that are common and significant to GBM, including both point mutations and CNVs. Thus, much of the most important diagnostic information can be derived from a very limited amount of input tissue, which is vital when biopsy material is limited.

Previous studies have highlighted the rates of specific mutations in GBM [3,35], but variant correlations were mainly restricted to activating mutations in *IDH* and the *TERT* promoter. Here, we have shown that cases with and without *EGFR* amplifications have distinct mutational profiles. Most

of the variants identified in this study were well known in the setting of GBM, but their enrichment within *EGFR*-amplified versus unamplified specimens may not have been appreciated (Fig. 2, Table 2).

*EGFR* amplification was recognized as a significant prognosticator in previous studies, but we found that *EGFR*-amplified cases were enriched in a population of patients with longer OS despite noted events of radiographic progression. *EGFR*-unamplified cases were split between the longer- and shorter-lived groups, but we were not able to identify any features to explain this disparity. The fact that some patients survived longer despite radiological evidence of disease progression begs the question as to whether these were true progression events versus pseudoprogression (ie, radiation necrosis). The lack of histological confirmation remains a limitation of this study and makes it an intriguing observation at this point. If confirmed in larger studies, it would be worthwhile to pursue an understanding of the underlying mechanisms.

It is clear from our work that particular combinations of mutations are found together in the setting of GBM and that some of these may correlate with longer OS. Because of the linked nature of the variants, we cannot determine which is actually responsible for the noted outcomes in the current dataset. Although this study highlights the clinical utility of concise NGS diagnostic panels, a broader platform (ie, whole-exome or -genome sequencing) and larger sample will be required to further explore the hypotheses outlined here.

## Supplementary data

Supplementary data to this article can be found online at https://doi.org/10.1016/j.humpath.2018.12.004.

## Acknowledgments

The authors gratefully acknowledge the contributions of the GPS@WUSTL team, who performed initial analyses of the cases used in this study, as well as the Washington University Cytogenetics and Molecular Pathology Laboratory where the FISH and IHC assays were performed and the Washington University Division of Neuropathology where morphological assessments were performed. We also thank Yu Tao and Jingqin Luo from the Siteman Biostatistics Shared Resource group for assistance with survival analyses.

## Author contributions

S. N. M., C. E. C., and S. D. designed the study. S. N. M., C. E. C., J. H. C., J. W. H., G. A., and S. D. acquired and analyzed the data. K. A. V. C. assisted in figure preparation. S. N. M. and S. D. wrote the manuscript.

## Ethical approval

This study was approved by the Institutional Review Board of the Washington University School of Medicine.

## References

[1] Ostrom QT, Gittleman H, Fulop J, et al. CBTRUS statistical report: primary brain and central nervous system tumors diagnosed in the United States in 2008-2012. Neuro Oncol 2015;17(Suppl. 4):iv1-iv62.
[2] Tanaka S, Louis DN, Curry WT, Batchelor TT, Dietrich J. Diagnostic and therapeutic avenues for glioblastoma: no longer a dead end? Nat Rev Clin Oncol 2013;10:14-26.
[3] Brennan CW, Verhaak RG, McKenna A, et al. The somatic genomic landscape of glioblastoma. Cell 2013;155:462-77.
[4] Eckel-Passow JE, Lachance DH, Molinaro AM, et al. Glioma groups based on 1p/19q, IDH, and TERT promoter mutations in tumors. N Engl J Med 2015;372:2499-508.
[5] Sturm D, Bender S, Jones DT, et al. Paediatric and adult glioblastoma: multiform (epi)genomic culprits emerge. Nat Rev Cancer 2014;14:92-107.
[6] Louis DN, Perry A, Reifenberger G, et al. The 2016 World Health Organization classification of tumors of the central nervous system: a summary. Acta Neuropathol 2016;131:803-20.
[7] Killela PJ, Reitman ZJ, Jiao Y, et al. TERT promoter mutations occur frequently in gliomas and a subset of tumors derived from cells with low rates of self-renewal. Proc Natl Acad Sci U S A 2013;110:6021-6.
[8] Quan AL, Barnett GH, Lee SY, et al. Epidermal growth factor receptor amplification does not have prognostic significance in patients with glioblastoma multiforme. Int J Radiat Oncol Biol Phys 2005;63:695-703.
[9] Hartmann C, Hentschel B, Simon M, et al. Long-term survival in primary glioblastoma with versus without isocitrate dehydrogenase mutations. Clin Cancer Res 2013;19:5146-57.
[10] Tini P, Cerase A, Cevenini G, Carbone SF, Miracco C, Pirtoli L. Epidermal growth factor receptor expression may correlate with survival through clinical and radiological features of aggressiveness in glioblastoma treated with radiochemotherapy. Anticancer Res 2015;35:4117-24.
[11] Labussiere M, Boisselier B, Mokhtari K, et al. Combined analysis of TERT, EGFR, and IDH status defines distinct prognostic glioblastoma classes. Neurology 2014;83:1200-6.
[12] Kessler T, Sahm F, Sadik A, et al. Molecular differences in IDH wildtype glioblastoma according to MGMT promoter methylation. Neuro Oncol 2018;20:367-79.
[13] Louis DN, Ohgaki H, Wiestler OD, et al. The 2007 WHO classification of tumours of the central nervous system. Acta Neuropathol 2007;114:547.
[14] Cottrell CE, Al-Kateb H, Bredemeyer AJ, et al. Validation of a next-generation sequencing assay for clinical molecular oncology. J Mol Diagn 2014;16:89-105.
[15] Li H, Handsaker B, Wysoker A, et al. The Sequence Alignment/Map format and SAMtools. Bioinformatics 2009;25:2078-9.
[16] Li H. A statistical framework for SNP calling, mutation discovery, association mapping and population genetical parameter estimation from sequencing data. Bioinformatics 2011;27:2987-93.
[17] Koboldt DC, Zhang Q, Larson DE, et al. VarScan 2: somatic mutation and copy number alteration discovery in cancer by exome sequencing. Genome Res 2012;22:568-76.
[18] McKenna A, Hanna M, Banks E, et al. The Genome Analysis Toolkit: a MapReduce framework for analyzing next-generation DNA sequencing data. Genome Res 2010;20:1297-303.
[19] Hagemann IS, Devarakonda S, Lockwood CM, et al. Clinical next-generation sequencing in patients with non–small cell lung cancer. Cancer 2014;121:631-9.
[20] Lek M, Karczewski KJ, Minikel EV, et al. Analysis of protein-coding genetic variation in 60,706 humans. Nature 2016;536:285-91.

[21] Talevich E, Shain AH, Botton T, Bastian BC. CNVkit: genome-wide copy number detection and visualization from targeted DNA sequencing. PLoS Comput Biol 2016;12:1-18.
[22] Kuilman T, Velds A, Kemper K, et al. CopywriteR: DNA copy number detection from off-target sequence data. Genome Biol 2015;16.
[23] Vlassenbroeck I, Califice S, Diserens AC, et al. Validation of real-time methylation-specific PCR to determine O6-methylguanine-DNA methyltransferase gene promoter methylation in glioma. J Mol Diagn 2008; 10:332-7.
[24] Furnari FB, Fenton T, Bachoo RM, et al. Malignant astrocytic glioma: genetics, biology, and paths to treatment. Genes Dev 2007;21:2683-710.
[25] Robinson GW, Orr BA, Gajjar A. Complete clinical regression of a BRAF V600E-mutant pediatric glioblastoma multiforme after BRAF inhibitor therapy. BMC Cancer 2014;14:258.
[26] Dahiya S, Emnett RJ, Haydon DH, et al. BRAF-V600E mutation in pediatric and adult glioblastoma. Neuro Oncol 2014;16:318-9.
[27] Forbes SA, Beare D, Gunasekaran P, et al. COSMIC: exploring the world's knowledge of somatic mutations in human cancer. Nucleic Acids Res 2015;43:D805-11.
[28] Cerami E, Gao J, Dogrusoz U, et al. The cBio cancer genomics portal: an open platform for exploring multidimensional cancer genomics data. Cancer Discov 2012;2:401-4.
[29] Gao J, Aksoy BA, Dogrusoz U, et al. Integrative analysis of complex cancer genomics and clinical profiles using the cBioPortal. Sci Signal 2013;6:pl1.
[30] Wick W, Weller M, van den Bent M, et al. MGMT testing—the challenges for biomarker-based glioma treatment. Nat Rev Neurol 2014;10: 372-85.
[31] Aldape K, Zadeh G, Mansouri S, Reifenberger G, von Deimling A. Glioblastoma: pathology, molecular mechanisms and markers. Acta Neuropathol 2015;129:829-48.
[32] Sottoriva A, Spiteri I, Piccirillo SG, et al. Intratumor heterogeneity in human glioblastoma reflects cancer evolutionary dynamics. Proc Natl Acad Sci U S A 2013;110:4009-14.
[33] Abou-El-Ardat K, Seifert M, Becker K, et al. Comprehensive molecular characterization of multifocal glioblastoma proves its monoclonal origin and reveals novel insights into clonal evolution and heterogeneity of glioblastomas. Neuro Oncol 2017;19:546-57.
[34] Sanson M, Marie Y, Paris S, et al. Isocitrate dehydrogenase 1 codon 132 mutation is an important prognostic biomarker in gliomas. J Clin Oncol 2009;27:4150-4.
[35] Crespo I, Vital AL, Gonzalez-Tablas M, et al. Molecular and genomic alterations in glioblastoma multiforme. Am J Pathol 2015;185: 1820-33.